Wavelet Graph Searches for Gravitational Chirps

Eve Chase

College of William & Mary, Williamsburg, Virginia

AstroParticule et Cosmologie, Paris, France

August 12, 2014

Abstract

As gravitational wave detector sensitivity increases with second generation detectors, direct detection of gravitational waves is increasingly more probable, with gravitational chirps from inspiraling merges between black hole and/or neutron star as the most probable source. Robust, efficient, and accurate data analysis methods are required to detect gravitational chirps. We provide a method for the production of a combined graph, representing numerous possible gravitational chirps within a wide range of times of coalescences and masses of the binary components. Interferometer data is searched along the directions of chirps in the graph, to locate gravitational chirps in transient oscillatory signals, in hopes of making the first direct detection of gravitational waves.

1 Introduction

1.1 Gravitational waves

Einstein's General Theory of Relativity spurred a scientific revolution, still thriving nearly a century later, with hopes of exploring the universe through the eyes of gravitational waves. Einstein's equations establish the dynamics of space-time, a mathematical model combining the dimensions of space and time. General relativity predicts the existence of gravitational waves, propagating disturbances of space-time. Gravitational waves are transverse waves traveling at the speed of light, produced by non-spherically symmetric accelerating masses.

The Hulse-Taylor binary (PSR B1913+16) provides substantial evidence for the existence and indirect observation of gravitational waves (Weisberg, Nice, & Taylor 2010). Consisting of a pulsar and companion neutron star, the Hulse-Taylor binary exhibits a gradual decrease in orbital period, following Einstein's predictions under the assumption that the system loses energy through the production of gravitational waves.

Despite the Hulse-Taylor binary's indirect evidence, gravitational waves have never been directly detected. A network of ground-based interferometers have been constructed for the purpose of making the first direct detection of gravitational waves (Figure 1). All detectors consist of two orthogonal arms of equal distance. Two identical laser beams travel over a supposedly-equal distance in their respective arms. The beams are recombined, producing an analyzable interference pattern. If a gravitational wave is passing through the detector, the two arms may have slightly different lengths, resulting in a phase difference in the two returning laser beams. This phase difference provides information about the nature of the gravitational wave. Using a network of several detectors allows for the elimination of noise sources and anomalies present in only one detector and allows for the location of gravitational wave sources through triangulation. At first generation sensitivity restrictions, detection is improbable. After the upgrades of second generation detectors, a ten-fold increase in sensitivity is expected, in addition to a higher detection probability (Chassande-Mottin 2013).

Figure 1: Location of current and future first and second generation gravitational wave detectors. First generation detectors are LIGO Hanford, LIGO Livingston, Virgo, and GEO 600. Second generation detectors are KAGRA, the proposed LIGO India, and advanced versions of the first generation detectors. Credits: Shawhan 2012

Gravitational waves are produced by a plethora of astrophysical sources. A gravitational core collapse star with non-axisymmetry is one such source of gravitational waves. A rotating star that lacks spherical symmetry, such as a newly-formed neutron star, produces gravitational waves as it becomes increasingly symmetric. Neutron star quakes, in which a disruption in the stellar magnetic field excited vibrational normal modes, are an additional potential source (Chamel & Haensel 2008). Due to instrument sensitivity limitations and low probability of a high energy gravitational wave to be produced within reasonable proximity to Earth, it is unlikely for the previously mentioned as-

trophysical scenarios to lead to gravitational wave detections. On the contrary, Compact Binary Coalescences (CBCs) are likely candidates for detection with second generation instruments, with an event rate of roughly forty per year (Sathyaprakash & Schutz 2009).

CBCs involve binary systems consisting of two compact objects, typically neutron stars and/or black holes, spiraling towards one another. As the objects inspiral, gravitational waves are produced with increasing energy and frequency, following a power law, until the compact objects are only a small distance apart. This signature increase in frequency is referred to as a chirp signal. Once the objects merge, the system enters a difficult to model ring down phase, resulting in the formation of a black hole. During the ring down phase, gravitational waves are produces as the resultant black hole radiates away its asymmetry. The system then reaches a state of equilibrium with little gravitational wave production.

Detecting gravitational chirp signals from CBCs requires highly sensitive detectors and precise data analysis methods.

1.2 Searches for gravitational wave transients

We detect gravitational chirps with the coherent WaveBurst (cWB) pipeline, a general search pipeline for the detection of gravitational wave transients. Through cWB, transient oscillatory signals in interferometer data are analyzed through a Wilson-Daubechiers Meyer (WDM) transform. The Wilson-Daubechiers transform superimposes signals into a time-frequency grid, with each gridpoint corresponding to a specific Meyer wavelet. A wavelet is an oscillation similar to a wave, with an amplitude that begins at zero, increases, and then decreases back to zero. Each wavelet is associated with a coefficient, correlating to its likelihood of being in a clustered pattern. Gravitational chirps provide identifiable signals in a WDM transform, through clusters of high coefficient wavelets following a power law in the time-frequency domain.

A given wavelet has a certain timescale. Timescale is analogous to resolution, allowing increased accuracy in time measurement with less accuracy in frequency measurement, or the opposite (Figure 2). Timescale is in units of time. At any given point in time, a chirp signal has an associated frequency and timescale. This results in a one-dimensional path in the three-dimensional space defines by timescale, time, and frequency.

1.3 Motivation

We seek to find an efficient, computationally inexpensive method of locating gravitational chirps in transient oscillatory signals within interferometer data. We produce possible chirp paths on a cWB grid and search along such paths for high WDM coefficients, suggesting the presence of a gravitational chirp.

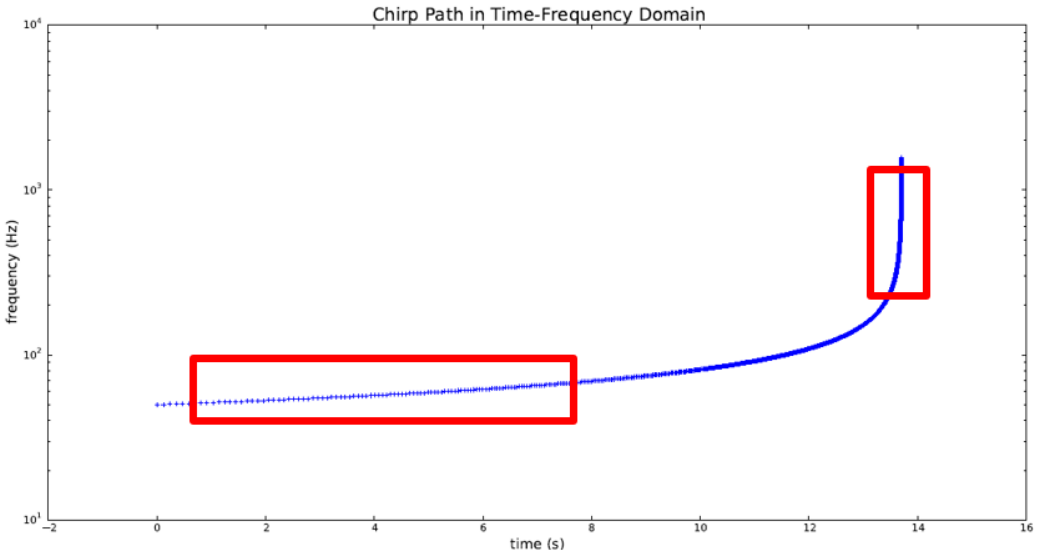

Figure 2: For any given gravitational chirp path in the time and frequency domain, the path will have a larger timescale at larger times, to provide greater frequency resolution, and smaller timescale at smaller times, to provide greater time resolution. This allows for efficient sampling and analysis of a chirp signal.

2 Construction and compilation of discrete chirp paths

We provide a method for the calculation of a set of possible gravitational chirp paths to be compared to interferometer data in a search for gravitational chirps. Chirp paths vary as a function of several parameters such as the time of coalescence and mass of the binary components, resulting in numerous possible paths. Ideally, we would search the interferometer data for every possible individual chirp path, but under the constraints of computational expenditure, we provide a different method. We calculate a series of possible chirp paths and combine all paths onto a single graph. We search interferometer data for large WDM coefficients along such constrained paths.

We first describe two models supporting the computation of continuous chirp paths in an infinite time-timescale-frequency space. We then provide a method for the digitization of each chirp path, in accordance with a cWB grid. In Sec. 2.4, we discuss the process of merging all paths onto a single graph.

2.1 Computing chirp paths

We discuss the computation of two chirp path models. First, we provide a simpler and less-precise Newtonian model. We then introduce a higher order

post-Newtonian model, using existing CBC pipelines.

2.1.1 Analytical approximation of Newtonian chirps

A continuous chirp path is sampled at a series of evenly spaced frequencies between a provided minimum and maximum. While the minimum frequency is constant for all mass pairs in a single search, maximum frequency varies for different masses. We use the frequency at the last stable orbit, the distance between stars at which the objects begin to merge, as the maximum frequency (Sathyaprakash & Schutz 2009). The frequency at the last stable orbit, normalized to a binary of mass $20M_{\odot}$, is

$$f_{LSO} \sim 220 \left(\frac{20M_{\odot}}{M}\right) Hz, \tag{1}$$

where M is the total mass of the binary. It is possible that a binary's maximum frequency may be less than the designated minimum frequency. For example, a 50-50$M_{\odot}$ binary will have a maximum frequency of 44 Hz, which is lower than the possible provided minimum frequency of 50 Hz. In this situation, a chirp path is not computed, and the binary is disregarded.

For each sampled frequency value, we calculate the associated timescale and time value indicative of a gravitational chirp following the stationary phase approximation (Dal Canton et al. 2014):

$$t(f) = \frac{1}{2\pi}\dot{\psi}(f) \tag{2}$$

$$s_t(f) = \sqrt{\left|\frac{\ddot{\psi}(f)}{2}\right|}, \tag{3}$$

where t is a time value and s_t is a timescale value, given a certain frequency. The phase, ψ is

$$\psi(f) = \frac{3}{128}\left(\zeta f\right)^{-5/3}, \tag{4}$$

where ζ is the following constant:

$$\zeta = \frac{\pi G\mathcal{M}}{c^3}. \tag{5}$$

$\mathcal{M}$ is the chirp mass, a mass which describes a binary system, calculated by

$$\mathcal{M} = \frac{(m_1 m_2)^{3/5}}{(m_1 + m_2)^{1/5}}, \tag{6}$$

where m_1 and m_2 are the masses of the individual stars composing the binary. In Equation 2, $\dot{\psi}$ is the first frequency derivative of ψ, and, in Equation 3, $\ddot{\psi}$ is the second frequency derivative.

Frequency is sampled in regular intervals, with an associated time and timescale value calculated for each sampled frequency. The interval at which frequency is sampled must be sufficiently small to ensure that the path can be properly analyzed. Therefore, the step in frequency sampling is

$$\Delta_f = \frac{1}{4s_t}, \tag{7}$$

where s_t is the timescale at the minimum frequency, which is found by substituting the minimum frequency into Equation 3.

By following this procedure, we compute a chirp path analytically, resulting in a set of timescale, time, and frequency coordinates at evenly sampled frequency values between a set minimum and maximum for any binary mass.

2.1.2 Numerical calculation of post-Newtonian approximations

The more precise post-Newtonian model is calculated in a similar manner to the Newtonian chirp model. Phase and frequency, which is directly related to phase, are calculated through the PyCBC python module, a Python toolkit for gravitational wave programs involving CBCs. For each phase corresponding to a frequency in range, corresponding time and timescale values are calculated following Equations 2 and 3, respectively.

We tested the post-Newtonian model with a TaylorF2 frequency domain template and produce chirp paths closely resembling the Newtonian chirp for identical binary component masses.

2.2 Digitization of path

2.2.1 Presentation of cWB grid

Coherent WaveBurst (cWB) requires that, in order to search input data from a gravitational wave detector for a proposed chirp signal, the chirp path must first be superimposed onto a cWB grid. This digitization process moves each sample of a continuous chirp path onto the closest grid bin, given a timescale, time, and frequency coordinate value. The number of time and frequency bins is dependent on the timescale, with higher frequency resolution (more bins) at high timescale and higher time resolution at low timescale (Figure 4). At a given timescale, the number of time and frequency bins are given by:

$$\text{time bins} = \frac{T}{s_t} - 1 \tag{8}$$

$$\text{frequency bins} = s_t f_s, \tag{9}$$

where T is the duration of the chirp, in seconds, and s_t is the timescale, in seconds. The sampling frequency, f_s, is the number of samples taken of the signal, per second. The intervals between successive bins is as follows:

$$\text{step in time} = s_t \tag{10}$$

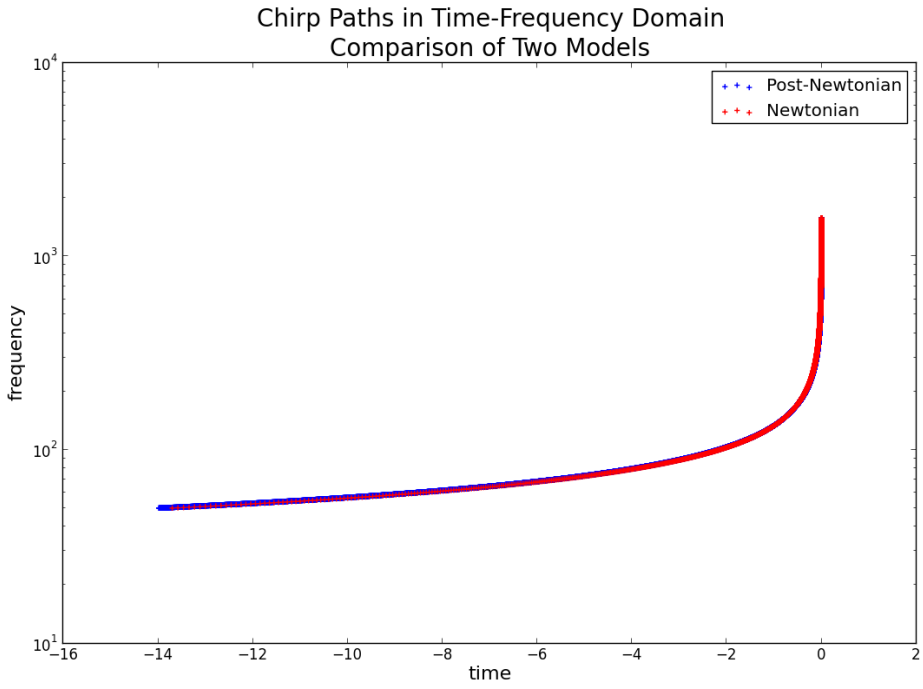

Figure 3: Newtonian and post-Newtonian models for chirp path calculation.

$$\text{step in frequency} = \frac{1}{2s_t}. \tag{11}$$

2.2.2 Digitization of path onto cWB grid

A cWB grid specifies a certain sampling frequency, duration, and set of timescale values. All other relevant information about the grid is extrapolated from these values. A chirp signal is initially computed without considering the cWB grid. A sampled chirp signal, with steps in frequency significantly smaller than that of the largest timescale, will have each sampled point sorted into its closest grid bin. First, a sampled continuous point is sorted into its closest timescale plane, while initially leaving the time and frequency coordinates unchanged. Timescale values are consecutive powers of two between some minimum and maximum value. If the unbinned coordinate's timescale value is smaller than the minimum allowed by the grid, then the value is reassigned to be this minimum possible timescale. A similar procedure is applied if the unbinned coordinate's timescale value is greater than the maximum dictated by the grid. If a timescale value is within the range allowed by the grid, the reassigned timescale index is

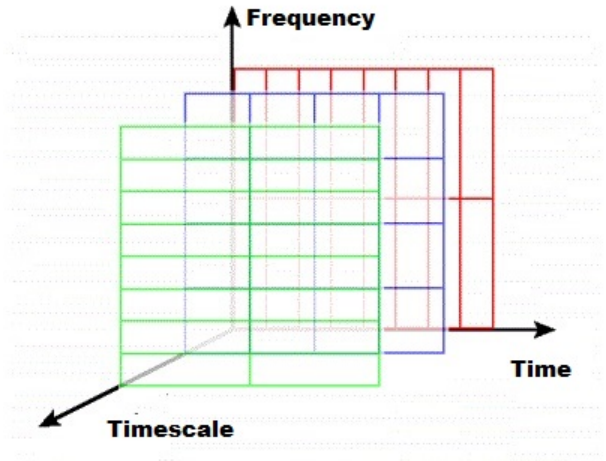

Figure 4: A three-dimensional representation of the cWB grid. At a higher timescale, there are more frequency bins and fewer time bins. The opposite is true for lower scale.

calculated by:

$$\text{timescale index} = \log_2 \frac{s_t}{s_{t,min}}, \tag{12}$$

where $s_{t,min}$ is the minimum timescale on the grid. Once a new timescale value is assigned, a coordinate is sorted into a specific time-frequency bin given the new timescale value. The binned time and frequency values are determined by reassigning each time and frequency value to the nearest increment of step size, as set by equations 10 and 11.

Figure 5 provides a graphical example of this "digitization" process. The cWB grid contains six occupied timescale exponents three through eight, corresponding to values from 2^3 to 2^8. Since the continuous curve contains many samples with timescales greater than the maximum of the grid, a significant portion of the digitized pixels occupy the maximum timescale plane. The larger step size in frequency at smaller timescales can be seen by the larger distance between digitized points at timescale exponent three as opposed to greater timescale exponents.

After the digitization of a single chirp path, we perform several more operations on the chirp path, detailed below, in order to properly identify gravitational chirps in the interferometer data.

2.3 Time shifts

When comparing multiple digitized chirp paths to find one that most matches the interferometer data, we must consider a range of possible chirp end times.

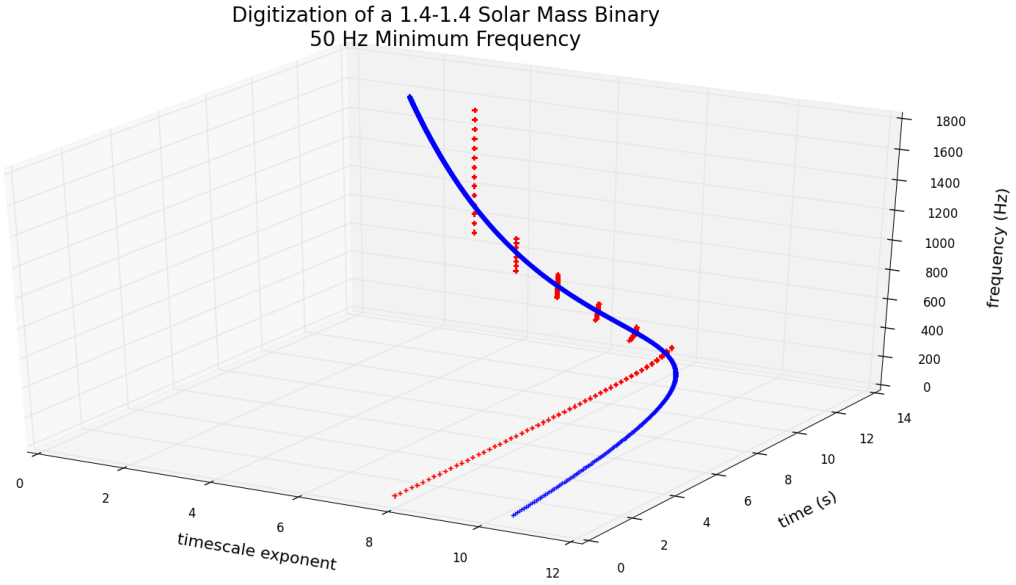

Figure 5: A continuous chirp path is digitized onto a cWB grid. The grid consists of six timescale planes. Many continuous chirp path coordinates had timescale values greater than the maximum timescale allowed on the grid, so several digitized coordinates are placed in this largest timescale plane. Frequency ranges from an inputted frequency of 50 Hz to the LSO frequency.

This is achieved by shifting each continuous chirp path in time, prior to digitization. Each time-shifted continuous path is digitized independently of the other chirp paths. Each chirp path is time-shifted in increments of half the minimum timescale ($\frac{s_{t,min}}{2}$) up to the maximum timescale. Figure 6 shows a time-shifted continuous chirp path and its original path. The time-shifted path will then be digitized and treated as a new chirp path, completely independent from the original chirp path that produced the shifted path.

2.4 Merging paths

After the computation of several digitized chirp paths, all paths are combined into one graph. Initially, each digitized path is handled individually. The digitized path is an ordered list of occupied cWB grid bins. Starting from the lowest time index present in the path, we record the timescale, time, and frequency coordinates for each occupied grid bin (node), in addition to the coordinates of the proceeding node, called an ancestor. A node can have multiple ancestors if

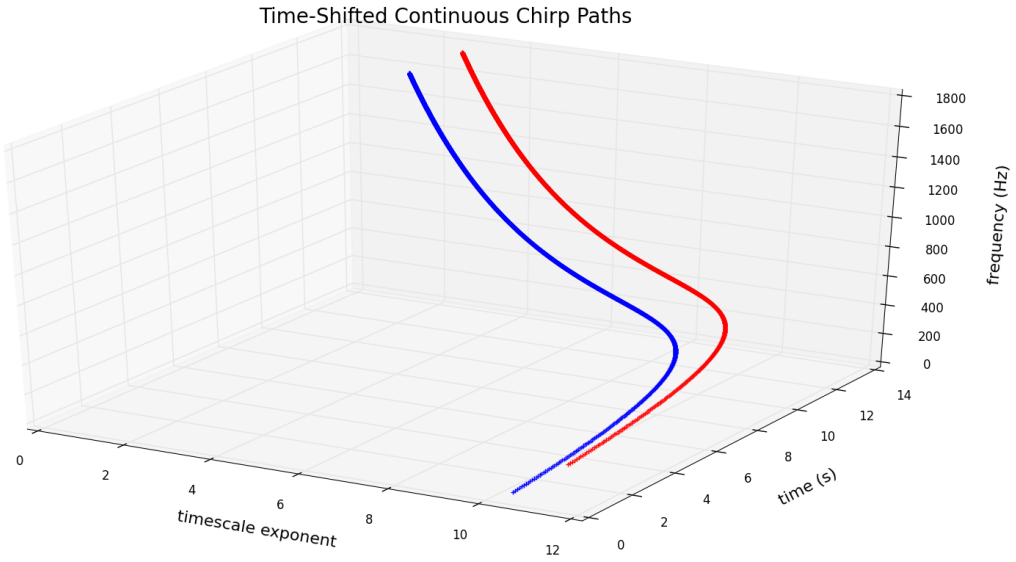

Figure 6: The maximum time-shift for a continuous chirp path.

the bin is occupied by multiple paths. All nodes are topologically sorted and plotted (Figure 7).

We plot each node by coordinate and color each node by either timescale exponent (Figure 7: top left, bottom left) or the number of ancestors (Figure 7: top right, bottom right). Many general trends are observed in merged path plots. A low number of connections is observed on frequency borders. At a given timescale, the bottom frequency nodes have no connections, since these are the first nodes in a path, and the top frequency nodes have few connections as they are typically not occupied by other paths. The high number of connections clustered at large times suggests a high density of paths near this time.

Merging all plots into one graph is a highly effective method of searching for gravitational chirps. Instead of individually searching interferometer data for one possible chirp at a time, we search for many chirps simultaneously by comparing this entire merged graph with interferometer data.

2.4.1 Alignment methods

Two different alignment methods are used during the production of a merged graph to provide better visualization for more effective analysis. Figure 7 represents a right-aligned graph, while Figure 8 is left-aligned. Both graphs use an

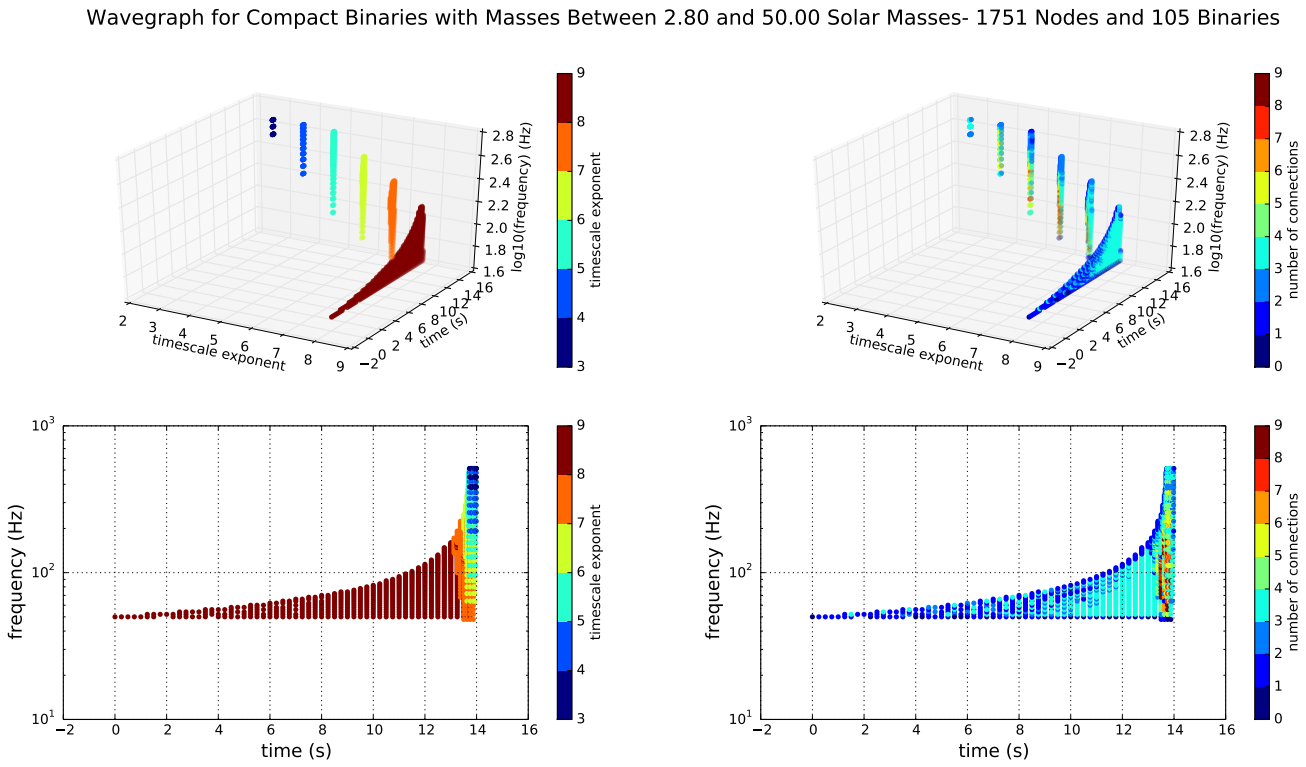

Figure 7: A plot of several hundred chirp paths, occupying 1751 cWB grid bins. The top left plot is a 3D representation of all nodes, colored by timescale. The top right plot is a 3D representation of all nodes, colored by number of connections. The bottom two plots are 2D projections in the time-frequency plane of the corresponding graphs above each.

identical set of input parameters and chirp paths.

The right-aligned plot requires that every chirp path end at the same time on the right. Therefore, the head node of each chirp path has the same time coordinate. We achieve this alignment by setting the smallest time index present in any chirp path to zero and shifting all other nodes by the following amount, given the node's coordinates of timescale, time, and frequency indices:

$$\text{new time index} = \text{old time index} - t_{min,index} 2^{s_{t,max} - s_t}, \tag{13}$$

where $t_{min,index}$ is the time index of the minimum time of all chirp paths, projected onto the maximum occupied timescale plane. In addition, $s_{t,max}$ is the index of the maximum occupied timescale plan and s_t is the timescale index of the node.

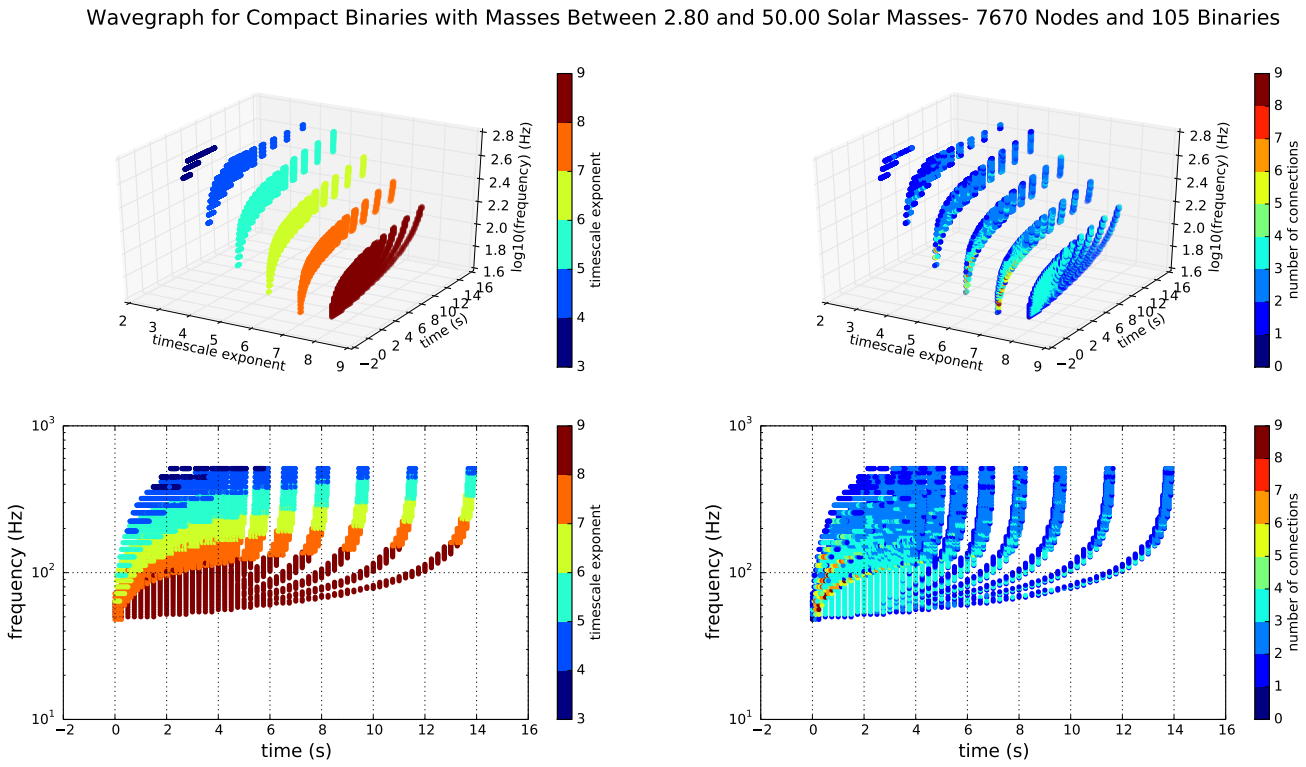

Figure 8: A left-aligned set of plots produced with an identical set of chirp paths and parameters to that of Figure 7.

Many more nodes are present in the left-aligned graph, since there is significant overlapping in the individual chirp paths for the right-aligned method.

The left-aligned plot requires that each continuous path start at time zero, before digitization. As a result, time-shifted paths will start at a time slightly after zero.

2.4.2 Chirp path computation models

We use a merged graph to visualize differences in the two models of chirp path computation: Newtonian, in Figure 9 and post-Newtonian, in Figure 10. Both graphs are produced with identical parameters. There are few differences in the two models; the original continuous chirp paths are slightly differently shaped, and there are differences in the number of connections.

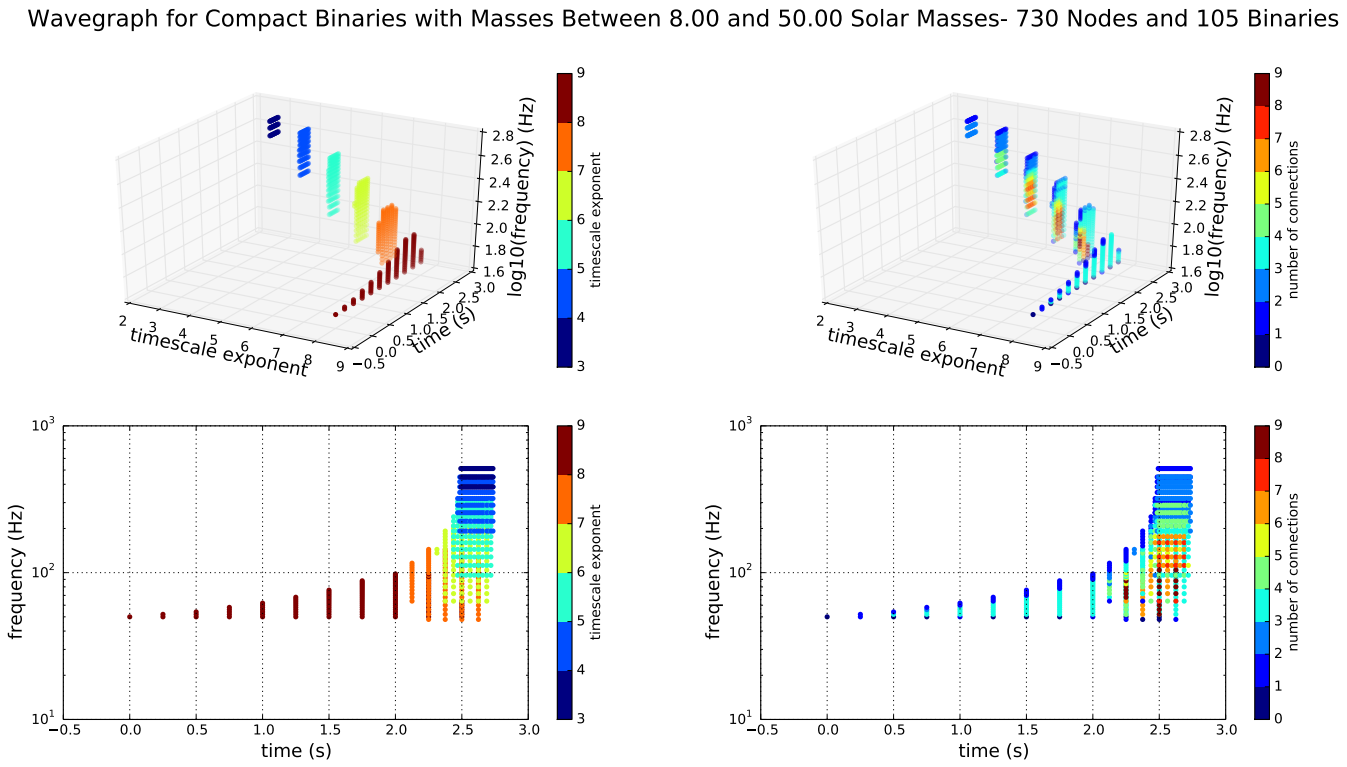

Figure 9: A merged graph of binaries from 4 - 4 $M_\odot$ to 25 - 25 $M_\odot$ with logarithmically selected masses and a Newtonian chirp path model.

2.4.3 Mass selection methods

We use two methods of binary mass pair selection between a specified minimum and maximum mass.

In the logarithmic sampling method, a specified number of masses are logarithmically selected between a minimum and maximum individual mass for a compact object making up the binary. From these logarithmically sampled masses, every possible unique combination of mass pairs is listed, including both symmetric and asymmetric pairs. For each pair, a chirp path is computed.

The use of a template grid provides a more exact method of mass pair selection, covering a more realistic and robustly sampled range of mass pairs. Given frequency and mass range restrictions, we use the PyCBC python module to produce a list of mass pairs.

Figure 10 is a merged grid produced with logarithmically sampled masses, while Figure 11 is produced with masses selected using the PyCBC template grid. Both graphs are produces with identical frequency parameters and a post-

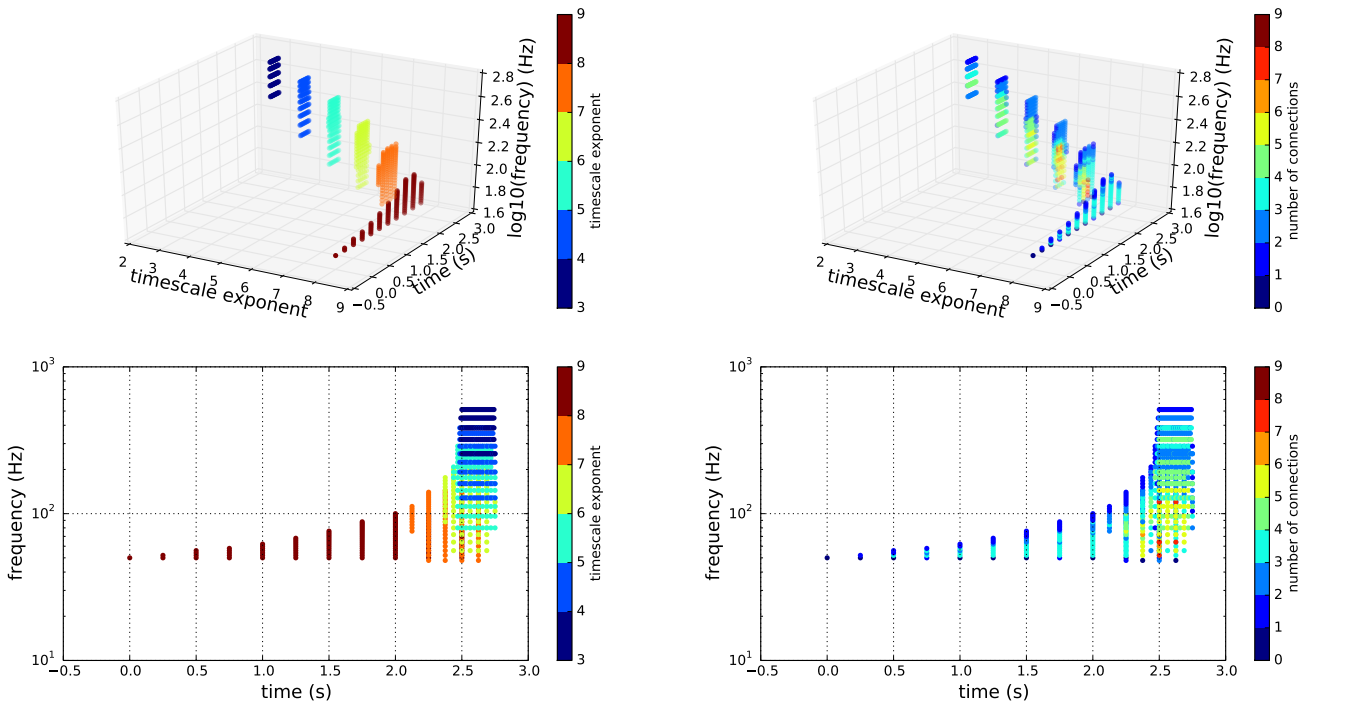

Figure 10: A merged graph of binaries from 4 - 4 $M_\odot$ to 25 - 25 $M_\odot$ with logarithmically selected masses and a post-Newtonian chirp path model.

Newtonian chirp path model. The template grid produces a greater number of connections clustered in the center of the cWB grid.

3 Conclusion

A method is provided for the production of a graph representing the combination of several possible gravitational chirp paths within a range of frequency and mass restrictions. Multiple methods are provided for chirp computation, graph alignment, and mass selection. This method will be included in a wavegraph production code with a broader purpose of searching interferometer data for gravitational chirps, in hopes of achieving the first direct detection of gravitational waves.

Acknowledgments

This work was supported by National Science Foundation award 1005036, through the University of Florida International REU for Gravitational

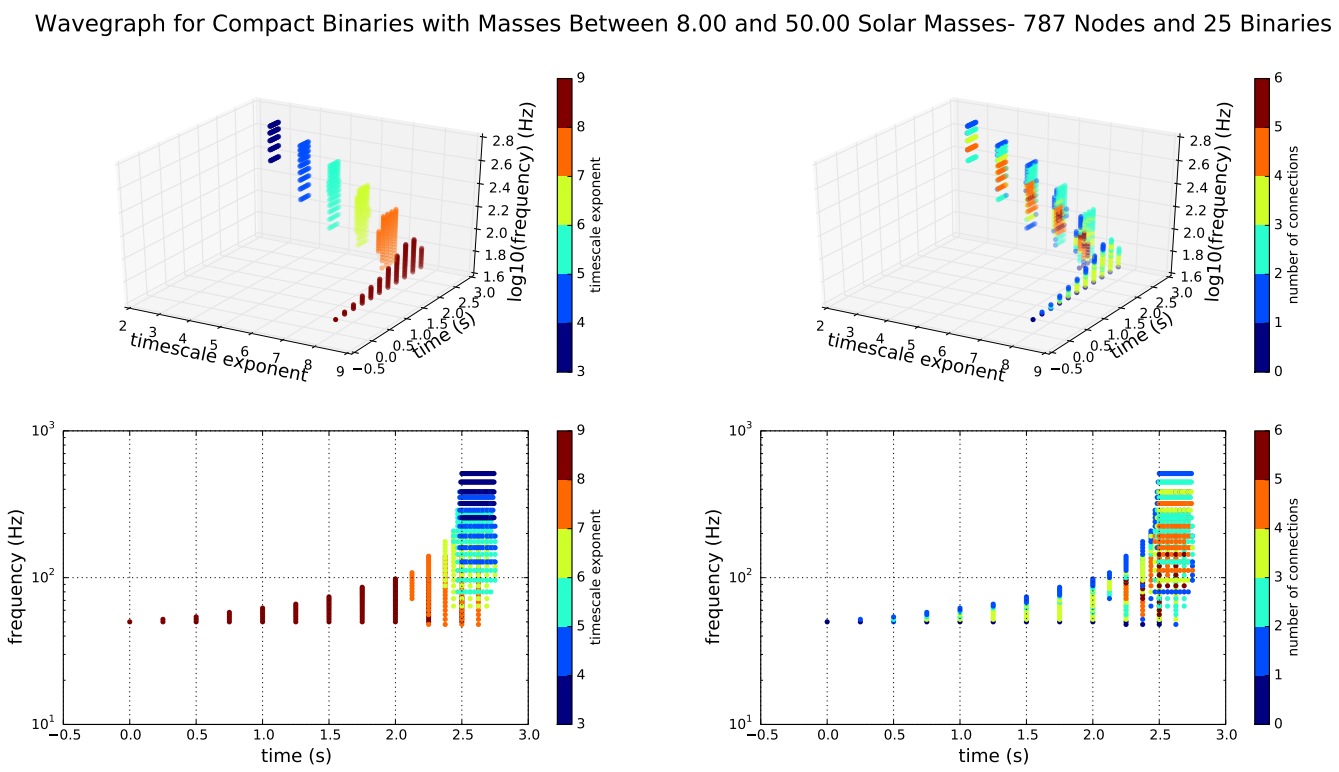

Figure 11: A merged graph of binaries from 4 - 4 $M_\odot$ to 25 - 25 $M_\odot$ with a post-Newtonian chirp path model and masses selected from a template grid.

Physics. My research progress and immense amount of technical skills gained would not be possible without the help of Eric Chassande-Mottin and Eric Lebigot. Thank you to all the friends I made at APC for making me feel welcome.

References

[1] Chamel, N. & P. Haensel. 2008, Living Rev. Relativity, 11, 10.

[2] Chassande-Mottin, E. 2013, AIPC, 1535, 252-259.

[3] Dal Canton, et al. 2014, Class. Quantum Grav., 31, 015016 (13pp).

[4] Riles, K. 2013, Progress in Particle & Nuclear Physics, 68, 1.

[5] Sathyaprakash, B.S. & B. F. Schutz. 2009, Living Rev. Relativity, 12, 2.

[6] Shawhan, P. 2012, SPIE, 8448, 844825.

[7] Weisberg, J.M., Nice, D.J., & J.H. Taylor. 2010, ApJ, 722: 1030-1034.